Supporting Information

Tixier et al. 10.1073/pnas.1301262110

SI Materials and Methods

Fly Stocks and Handling. All *Drosophila melanogaster* stocks were grown on standard medium and crosses were performed at 25 °C. The following strains were used: *MHC-tauGFP* (E. N. Olson and E. Chen, Medical Center at Dallas, Dallas, TX), *duf-Gal4* (gift of K. Vijayaraghavan, Tata Institute of Fundamental Research, India), *UAS-AMPK* (J. K. Chung, Korea Advanced Institute of Science and Technology, Republic of Korea), $AMPK^{\alpha 3}$ (V. Mirouse, Génétique Reproduction et Développement, Clermont-Ferrand, France), $Akt1^{9}$ (Y. N. Jan, Howard Hughes Medical Institute, San Francisco), Tor^{2L1} and $foxo^{25}$ (E. Hafen, Institute of Molecular Systems Biology, Zurich, Switzerland), $rictor^{\Delta 2}$ (S. M. Cohen, European Molecular Biology Laboratory, Heidelberg, Germany), and *UAS-Pten* (T. Xu, Yale University School of Medicine, New Haven, CT). The UAS-RNAi line for *Tor*, 5092R-2, comes from the NigFly collection, all other UAS-RNAi lines come from the Vienna Drosophila RNAi Center collection. The following RNAi lines have been used: 106818 for *Pglym78*, 105666 for *Pfk*, 25643 for *Tpi*, 100596 for *Gapdh1*, 110081 for *Pgk*, 49533 for Pyk, and 31192 for *Impl3*. For glycolytic gene knockdown experiments in developing muscles, the *duf-Gal4* or *Mef2-Gal4* driver lines were used. *duf-Gal4* is expressed exclusively in founder cells (FCs) and developing muscle precursors, not in fusion-competent myoblasts (FCMs) and in muscle precursors to which FCMs are going to fuse, whereas *Mef2-Gal4* is expressed in both types of cells. Both lines display similar expression pattern at stage 13 [9.5 h after egg laying (AEL)] when glycolytic genes start to be expressed. *M6-gapGFP* line was generated by R. Aradhya in the laboratory by injecting a modified *gapGFP* version of previously described M6-GFP construct (1).

The *Pglym78* deficiency line was obtained by using flippase recognition target-mediated recombination between the P(XP) $CG14516^{d10571}$ and PBac(WH)$ligatin^{f04182}$ lines (Exelixis, Harvard Medical School). All others were obtained from Bloomington *Drosophila* Stock Center.

Mutants were balanced using FM7c, P{*Act-LacZ*}, CyO, P{wg^{en11}-*LacZ*}, TM3, *Ser*, P{*twi-LacZ*}, and homozygotes were identified by the absence of LacZ staining.

dsRNA Injection. For each candidate gene, two distinct dsRNAs targeting all mRNA isoforms were produced. *MHC-tauGFP* embryos were aligned on a slide, covered with oil, injected as described previously (2), and examined after 16 h of development on a confocal miscroscope (Leica SP5). For each dsRNA at least 50 embryos were injected. Lethality and phenotypes were scored and data were considered as specific if muscular phenotypes were the same with the two dsRNAs for each gene and were observed in at least 25% of the embryos.

In Situ Hybridization and Immunostaining. Fluorescent in situ hybridization with the TSA amplification system (Perkin–Elmer) and immunohistochemistry were done as described previously (3). The Gold collection clones GH12192, GH10864, RE69448, GH07208, GH13304, SD06874, and RE54418 were used to generate RNA probes against glycolytic genes. For fluorescent staining, the following antibodies were used: guinea pig anti-Eve (1:1,000; D. Kosman, University of California, Los Angeles, CA), mouse anti-Lbe [1:2,500 (4)], rabbit anti–β-3 tubulin (1:5,000; R. Renkawitz-Pohl, Philipps University, Marburg, Germany), rat anti-actin (1:300, MAC 237; Babraham Bioscience Technologies), rabbit anti-LacZ (1:1,000; Sigma), mouse anti-Engrailed [1/200; Developmental Studies Hybridoma Bank (DSHB)], rabbit anti-Tinman (1/1000; M. Frasch, Erlangen University, Erlangen, Germany), mouse anti-Elav (1/200; DSHB), and mouse anti-Delta (1/100; DSHB). Cy3, Cy5, and 488 conjugated secondary antibodies were used (1:300; Jackson Immuno-Research). Embryos were mounted in anti-fade Fluoromount-G reagent (Southern Biotech). Labeled embryos were analyzed using an LSM510 Meta (Zeiss) confocal microscope, an SP5 RS MP (Leica) or SP8 (Leica) equipped with HyD detector, with a 40× objective. Images were processed with ImageJ and Photoshop.

Pyruvate Kinase Activity. *Drosophila* embryos were collected at the indicated time points and homogenized in five volumes of assay buffer with a dounce homogenizer. Samples were gently centrifuged and the supernatant was directly used for pyruvate kinase activity measurements with a pyruvate assay kit (K609-100; BioVision Research). The optical density at 570 nm (OD_{570nm}) of the assay reaction product was measured on a microplate reader (ThermoLabsystems). For each sample, protein concentration was determined with a Bradford assay.

Staging Embryos, Nuclei Counting, and Muscle Size Measurement. In addition to overall embryonic morphology, dorsal closure and gut morphology were used for precise staging of all embryos. To determine the number of nuclei in the dorsal acute 1 (DA1) and the segmental border muscle (SBM) muscles, *Drosophila* embryos were double-stained with anti–β-3 tubulin (to reveal all muscles) and with anti-Eve or anti-Lbe (to reveal DA1 or SBM nuclei, respectively). Nuclei were counted using a 40× objective on a LSM510 Meta (Zeiss) or on a SP5 RS MP (Leica) confocal microscope. For each muscle/mutant condition analyzed, 30 abdominal hemisegments of embryos at stage 15 were counted (minimum 10 embryos) (Table S2*A*). For the kinetics analyses, 20 hemisegments were counted at stage 12 (8 h AEL), 13 (9.5 h AEL), 14 (10.5 h AEL) and at early (11.5 h AEL) and late stage 15 (13 h AEL) (Table S2*B*). Data plots and statistical analyses were performed with Prism 5.0 using Kruskal–Wallis and Dunn's posttests.

DA1 and SBM size were measured with the Volocity software (Table S2*A*). Muscle width is a mean value from the measurements that were performed at three different points along the myotube to take into account the potential variations of muscle width. Data plots and statistical analyses were performed with Prism 5.0 using Student *t* test.

In each graph, columns correspond to the mean and error bars correspond to the SD. $^{***}P < 0.0001$, $^{**}0.001 < P < 0.01$; $^{*}0.01 < P < 0.05$.

Actin Foci and *M6-gapGFP* Positive Fusion-Competent Myoblast Counting. Actin foci and *M6-gapGFP*-positive FCM were counted using a 40× objective on a SP8 (Leica) confocal microscope. For each stage/mutant condition analyzed, 30 abdominal hemisegments were counted (Table S3). In each graph, columns correspond to the mean and error bars correspond to the SD. $^{****}P < 0.0001$.

Zebrafish Morpholino Design and Injections. The following morpholino oligonucleotides (GeneTools) were used for zebrafish experiments:

*pgam2*MO: ATGAAAAGGATATTTGGGTTTCACT, (target: *pgam2* ATG region)

misMO: ATCAAAACGATATTTCGGTATGACT, (five mismatch morpholino)

*p53*MO: GCGCCATTGCTTTGCAAGAATTG, (target: *p53*)

A reporter construct for testing knockdown specificity was generated by inserting the ATG region of *pgam2* (tactgtagtgaaaccaaatatccttttcata ATG GCT GCT GCT CAT CGT CTA GTG ATT GT) into the EcoRI/NcoI sites of the pCS2:GFP reporter vector (5).Morpholino oligonucleotides (*pgam2*MO) or (misMO) were coinjected with a morpholino targeting P53 (*p53*MO) to suppress unspecific morpholino-induced apoptosis (6) (Fig. S3). Immunohistochemistry with phalloidin and the F59 (mouse monoclonal antibody (7) that stains slow twitching muscle fibers in the zebrafish) and Pax7 antibodies was carried out as described (8).

The diameters of six fibers per segment were measured. The number of fibers in a 500- × 500-pixel square was counted and this was repeated eight times for each condition. To determine the number of nuclei per fiber, fibers were labeled with a Unc45-b-GFP fusion construct as described (9). Nine and 13 fibers were counted in misMO/*p53*MO-injected and in *pgam2*MO/*p53*MO-injected embryos, respectively. Data plots and statistical analyses were performed with Prism 5, using Mann–Whitney *U* test, Kruskal–Wallis test with Dunn's posttest (Fig. 3 *L–N*), and Fisher's exact test.

1. Rebeiz M, Reeves NL, Posakony JW (2002) SCORE: A computational approach to the identification of *cis*-regulatory modules and target genes in whole-genome sequence data. Site clustering over random expectation. *Proc Natl Acad Sci USA* 99(15): 9888–9893.
2. Kennerdell JR, Carthew RW (1998) Use of dsRNA-mediated genetic interference to demonstrate that frizzled and frizzled 2 act in the wingless pathway. *Cell* 95(7): 1017–1026.
3. Junion G, et al. (2007) Genome-wide view of cell fate specification: Ladybird acts at multiple levels during diversification of muscle and heart precursors. *Genes Dev* 21(23): 3163–3180.
4. Jagla T, et al. (1998) Ladybird determines cell fate decisions during diversification of Drosophila somatic muscles. *Development* 125(18):3699–3708.
5. Ertzer R, et al. (2007) Cooperation of sonic hedgehog enhancers in midline expression. *Dev Biol* 301(2):578–589.
6. Robu ME, et al. (2007) p53 activation by knockdown technologies. *PLoS Genet* 3(5):e78.
7. Crow MT, Stockdale FE (1986) Myosin expression and specialization among the earliest muscle fibers of the developing avian limb. *Dev Biol* 113(1):238–254.
8. Costa ML, Escaleira RC, Rodrigues VB, Manasfi M, Mermelstein CS (2002) Some distinctive features of zebrafish myogenesis based on unexpected distributions of the muscle cytoskeletal proteins actin, myosin, desmin, alpha-actinin, troponin and titin. *Mech Dev* 116(1-2):95–104.
9. Etard C, et al. (2007) The UCS factor Steif/Unc-45b interacts with the heat shock protein Hsp90a during myofibrillogenesis. *Dev Biol* 308(1):133–143.

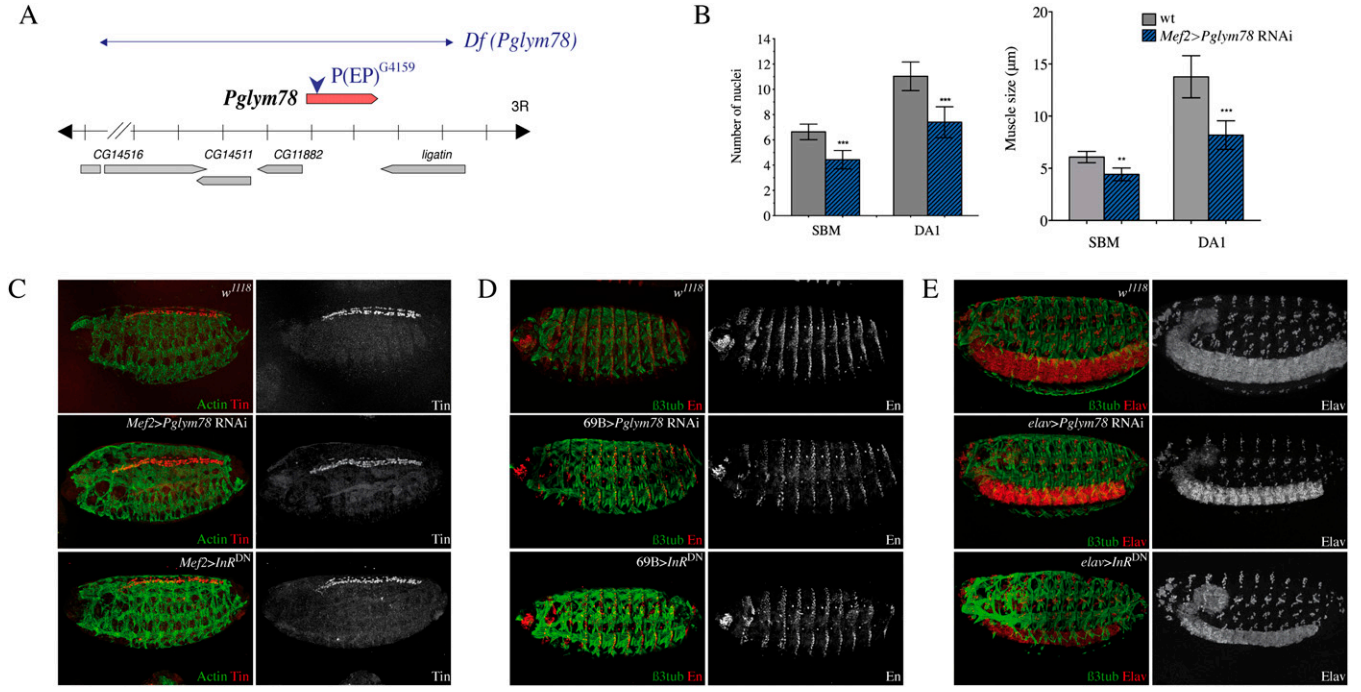

Fig. S1. *Pglym78* mutants and RNAi knockdown contexts. (*A*) Genomic map of the *Pglym78* locus showing the insertion point of the *P(EP)*^{G4159} element and the location of the generated deficiency *Df(Pglym78)*. (*B*) Number of nuclei and size of SBM and DA1 muscles in wildtype and in the *Mef2>Pglym78* RNAi context. Twenty muscles from abdominal segments A2–A5 in stage-15 embryos have been analyzed. SD is indicated. (*C–E*) Attenuation of *Pglym78* expression or insulin pathway knockdown have no effect on nonfusing tissues. *Pglym78* RNAi or InR^{DN} overexpression in heart (*C*), epidermis (*D*), or nervous system (*E*) do not affect developmental cell patterns of these tissues.

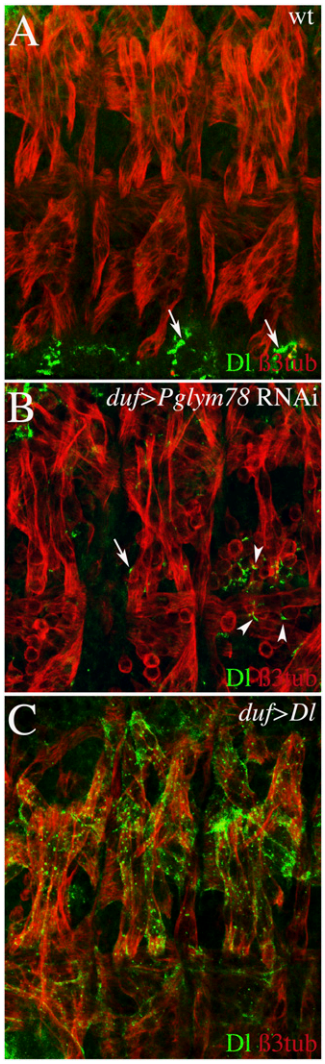

Fig. S2. Delta expression and function in developing muscles. (*A–C*) Lateral views of three abdominal segments from late stage-14 embryos (11 h AEL) stained for Delta (green) and β-3 tubulin (red) to reveal muscles. (*A*) In wild-type embryos Delta is detected in neural cells (arrowheads) but not in muscles. (*B*) In *Pglym78* RNAi context Delta is detected in unfused FCMs (arrowheads). Arrow points to a dotty Delta signal that occasionally appears in myotubes. (*C*) Ectopic expression of Delta in myotubes does not influence fusion.

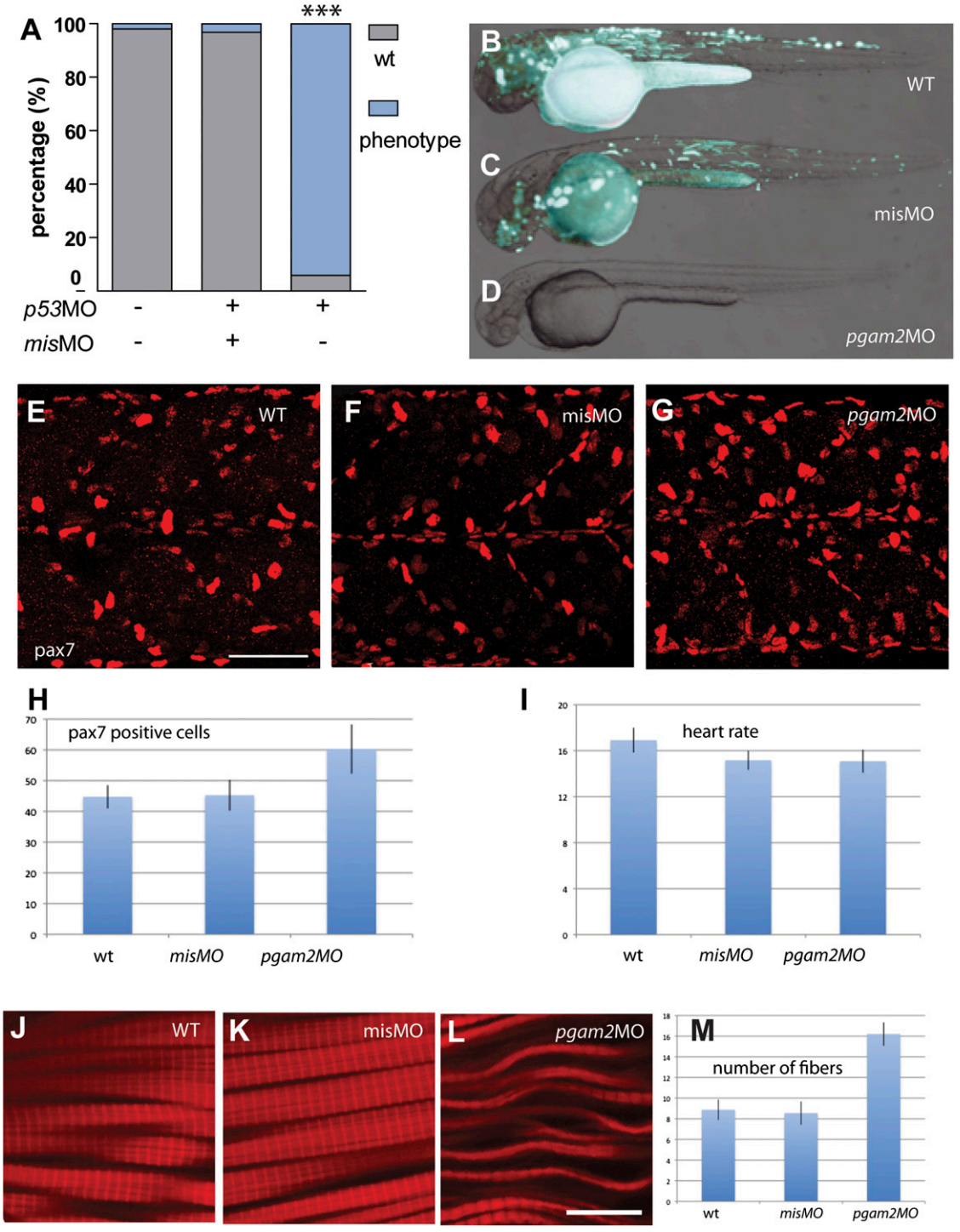

Fig. S3. Control morpholino experiments in zebrafish. (*A*) Percentage of larvae showing a reduction in birefringence (phenotype, blue) after injection of the indicated morpholinos (Fisher's exact test ; ***$P < 0.0001$). Injection of control morpholinos carrying five mismatches (misMO) does not lead to any obvious phenotype. (*B–D*) Coinjection of *pgam2* morpholino and a construct carrying a GFP reporter of *pgam2* expression revealed loss of GFP expression (*D*) compared with embryos only injected with the reporter construct (*B*) or to embryos coinjected with the mismatch morpholino (*C*). (*E–H*) Immunostaining against Pax7 revealed an increase of Pax7-positive nuclei in *pgam2* morphants (*G*) compared with uninjected (*F*) or control morpholino-injected embryos (*G*). (Scale bar: 47.5 μm.) (*H*) Quantification of Pax7-positive myoblasts. All nuclei were counted in an area of 500 × 500 pixels in 10 different 48 hours postfertilization (hpf) embryos for each category and summarized in a chart. (*I*) Rate of heart beat in 48 hpf embryos (counted during 10 s, $n = 12$ embryos for each category). (*J–M*) Immunostaining with phalloidin in (*J*) uninjected, (*K*) control morpholino-injected embryos, and (*L*) *pgam2* morphants; 48 hpf embryos. (Scale bar: 12 μm.) (*M*) Number of fibers present within a square of 500 × 500 pixels (eight squares counted for each category).

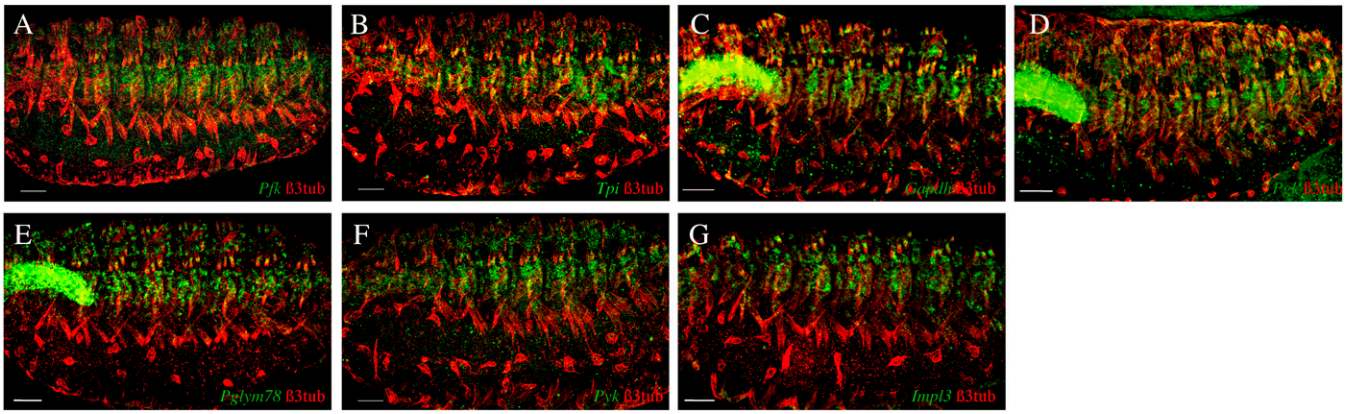

Fig. S4. Expression profiles of glycolytic genes and *Impl3*. (*A*–*G*) Lateral views of whole stage-15 (13 h AEL) embryos double-stained for glycolytic gene and *Impl3* transcripts (green) and for β-3 tubulin to reveal muscles (red). Note that all glycolytic genes and *Impl3* show predominantly muscular expression. (Scale bar: 30 μm.)

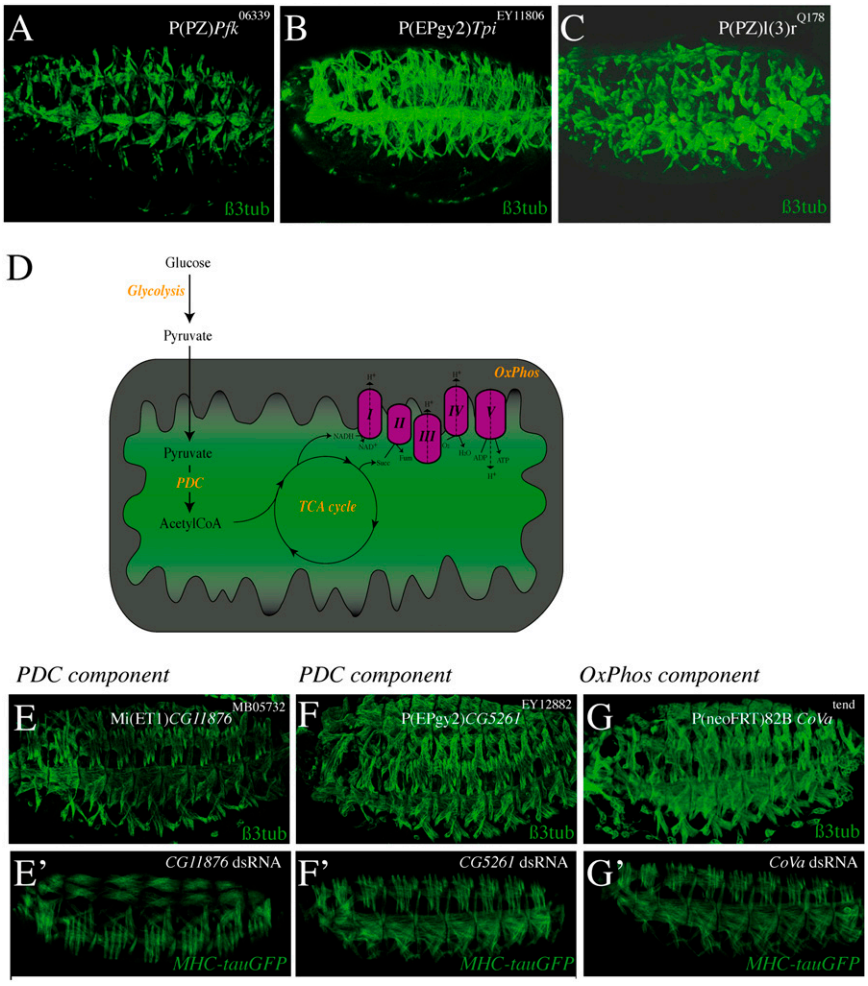

Fig. S5. Muscle phenotypes observed in different metabolic gene mutants. P element insertion mutants of *Pfk* (*A*), *Tpi* (*B*), and *Pyk* (*C*) display reduced size muscle phenotypes and unfused myoblasts. Especially for *Pyk* the observed phenotypes appear more severe than RNAi knockdown phenotypes (compare with Fig. 4). (*D*) Scheme showing conversion of pyruvate into AcetylCoA in mitochondria via the pyruvate dehydrogenase complex (PDC) and its trafficking through TCA cycle and oxidative phosphorylation (OxPhos). Mutant alleles and RNAi knockdown (by dsRNA injections into *MHC-tauGFP* embryos) of the pyruvate dehydrogenase complex components *CG11876* (*E and E'*) and *CG5261* (*F and F'*) and of the respiratory chain component *CoVa* (*G and G'*) reveal that loss of function of these genes does not affect muscle pattern. Lateral views of stage-15 embryos stained with anti–β-3 tubulin are shown.

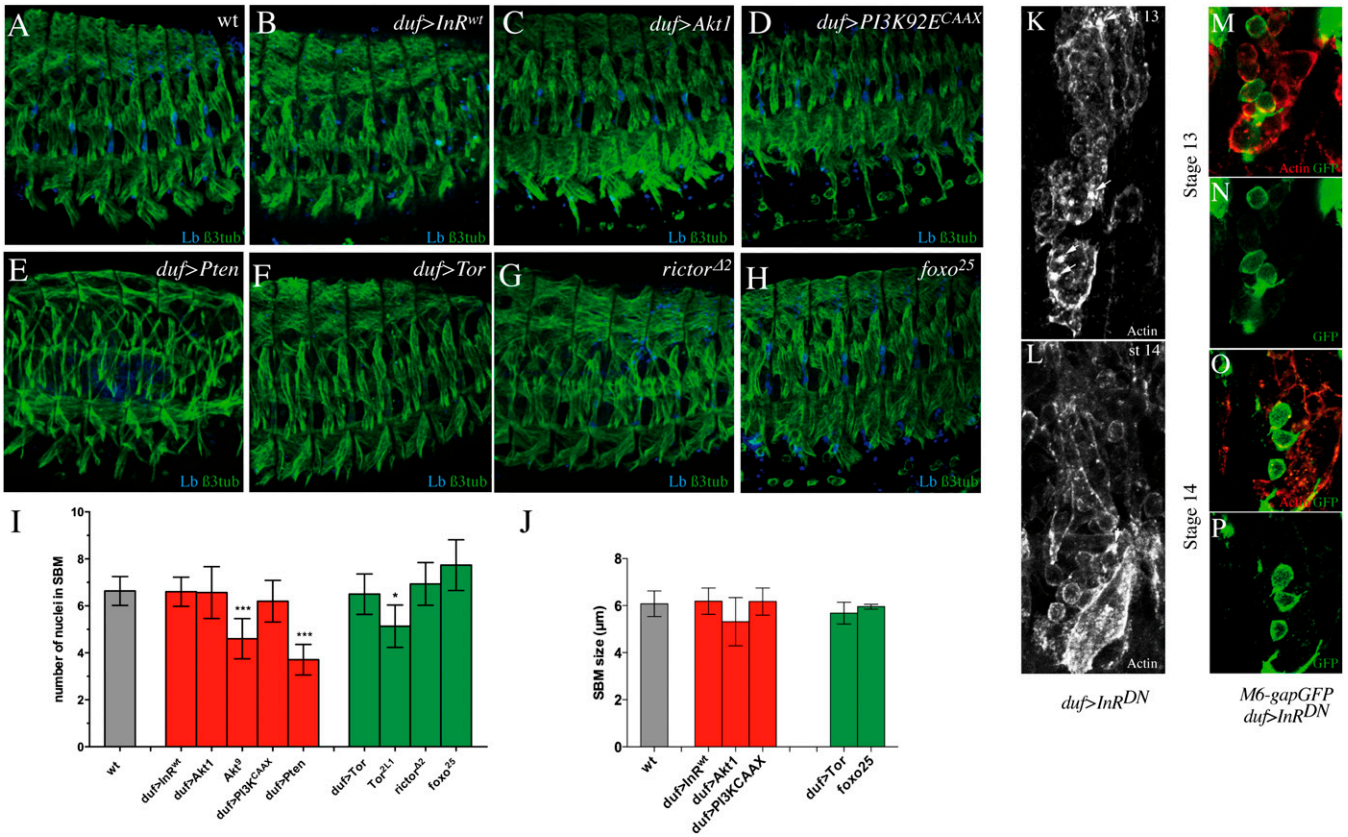

Fig. S6. Muscle phenotypes observed in different gain and loss of function contexts for insulin and TOR pathway components. Activation of the insulin pathway by muscle specific overexpression of *InR* (*B*), *Akt* (*C*), or *PI3K* (*D*) as well as the TOR pathway by overexpressing Tor (*F*) do not affect muscle pattern. Similarly, muscles appear normal in the *foxo* mutant (*H*). In contrast, the inactivation of the insulin pathway by muscle specific overexpression of *Pten* (*E*) leads to muscular defects. The absence of muscular defects in the *rictor* mutant compared with the Tor^{2L1} mutant (compare Fig. S6*G* with Fig. 5*E*) shows that only the activity of TORC1 is implicated in embryonic myogenesis. Lateral views of stage-15 embryos stained for β-3 tubulin (green) and Ladybird early (blue) are shown. Quantification of the number of nuclei in SBM (*I*) and of the size of SBM muscles (*J*) in genetic contexts shown in (*A*–*H*). Bar graphs show the mean number of nuclei or the mean muscle size ± SD and asterisks indicate significance of changes compared with the wildtype. (*K*–*L*) Appearance of actin foci (arrows) in developing muscles in ventro-lateral domain of stage-13 (*K*) and stage-14 (*L*) *duf* > InR^{DN} embryos. (*M*–*P*) Monitoring of *M6-gapGFP*–positive FCMs in stage-13 (*M* and *N*) and stage-14 (*O* and *P*) *duf* > InR^{DN} embryos.

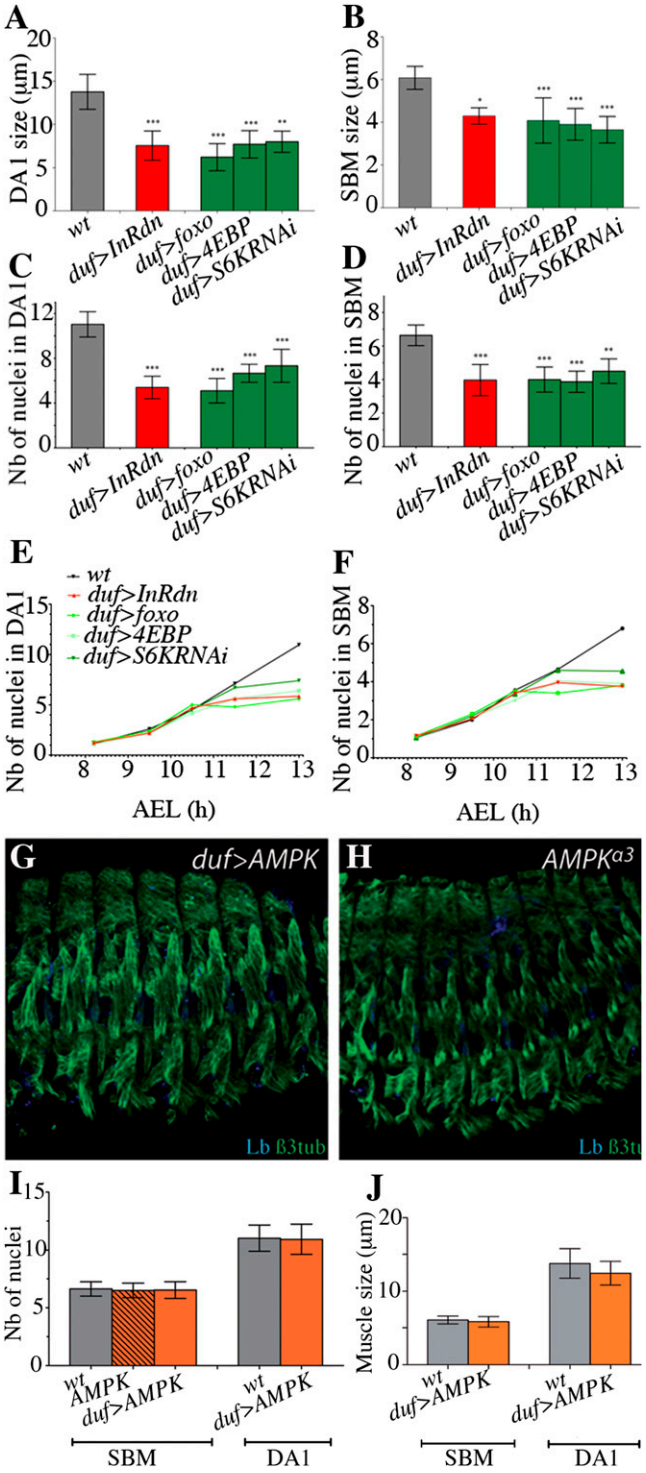

Fig. S7. Assessment of muscle phenotypes in embryos with affected insulin, Tor, and AMPK pathways. (*A* and *B*) Relative muscle size and (*C* and *D*) number of nuclei in DA1 and SBM muscles in stage-15 (13 h AEL) wild-type embryos (gray) and in embryos with affected insulin pathway (red) or overexpressing *foxo* or affected for the TOR pathway (green). (*E* and *F*) Kinetics of fusion in DA1 and SBM in the wildtype and in embryos with affected insulin or TOR pathway or overexpressing *foxo*. Mean values are used to visualize the number of nuclei according to time AEL. *(G–J) AMPK* loss of function or muscle-specific overexpression of AMPK does not affect muscle development in *Drosophila* embryos. (*G* and *H*) Muscle pattern of stage-15 embryos stained for β-3 tubulin (green) and Ladybird early (blue). (*G*) Embryos with muscle-targeted overexpression of *AMPK* and (*B*) $AMPK^{a3}$ mutants show nonaffected wildtype-like muscle pattern. (*I*) Number of nuclei present in DA1 and SBM in stage-15 embryos. (*J*) Muscle size of DA1 and SBM muscles. Bar graphs show the mean number of nuclei or mean size of muscles ± SD.

Table S1. List of identified *Drosophila* and zebrafish muscle genes

Table S1

First sheet: list of the 132/169 orthologs expressed in developing muscles in *Drosophila* and zebrafish, respectively. On red background are genes tested by dsRNA injections. Genes annotated by an asterisk correspond to candidates already known to be involved in myogenesis. Genes in bold are involved in glycolysis. Second and third sheets: list of all *Drosophila* and zebrafish genes expressed in developing embryonic muscles identified by screening BDGP and ZFIN expression databases. The following query terms were used for searching the Berkeley Drosophila Genome Project database: "somatic muscle primordium," "embryonic/larval muscle system," and "embryonic/larval somatic muscle" and for the Zebrafish Information Network database, "somites." Orange background denotes the genes that are conserved between the two species and expressed in muscle compartments. Green background highlights genes that are conserved but expressed in muscle in only one of the two species. Blue background denotes genes whose expression is not described in one of the two species, whereas on white background are genes that are not conserved.

Table S2. Quantification of muscle growth parameters

Table S2

Table S2*A* shows the number of nuclei and size of DA1 and SBM muscles in wild-type and in *Pglym78,* insulin, and TOR pathway mutant embryos at embryonic stage 15. For each genotype, the average number of nuclei ± SD is shown ($n = 30$). The number of nuclei in null mutant contexts was determined only in the SBM muscle. For each genotype, the average size in micrometers ± SD is shown ($n = 20$). Table S2*B* shows kinetics of the myoblast fusion process in the wild-type condition and in *Pglym78,* insulin, and TOR mutant conditions. For each stage and each genotype, the average number of nuclei ± SD is shown ($n = 20$).

Table S3. Quantification of actin foci and *M6-gapGFP*–positive FCMs

Table S3

For each stage and each genotype, the average number of foci or *M6-gapGFP* positive FCMs ± SD is shown ($n = 30$).